

ADAPTIVE WING FLUTTER SUPPRESSION BY MEANS OF MULTIPLE TRAILING EDGE CONTROL SURFACES - A COMPARATIVE STUDY

Vindigni C. R.*1, Mantegna G.1, Esposito A.1, Orlando C.1 & Alaimo A.1

¹Kore University of Enna, Department of Engineering and Architecture, Enna, Italy

Abstract

In this work the employment of multiple control surfaces for adaptive flutter suppression systems design of wings is addressed. The aeroelastic plant is modeled taking advantage of an aeroelastic beam finite element framework that relies on an equivalent beam idealisation of the structure and strip theory aerodynamics, including the dynamics of trailing edge control surfaces. A simple adaptive control architecture is employed to realize the flutter suppression systems and the passivity requirement of the aeroelastic plant is ensured by a parallel feedforward compensator implementation. Single and double aileron based flutter suppression systems are investigated and their performance are compared in terms of flutter boundary extension with respect to the open loop case.

Keywords: Wing flutter, Adaptive flutter suppression, aeroelastic beam

*Corresponding Author: Carmelo Rosario Vindigni

Kore University of Enna, Department of Engineering and Architecture, Enna, Italy E-mail: carmelorosario.vindigni@unikore.it

1. Introduction

Modern aircraft design is mainly focused on lightweight high aspect ratio wings for next generation aircrafts; in fact, reduced overall weight of the structure and higher aspect ratio are strictly related to a less fuel consumption, that is a key aspect in reducing CO2 emissions. However, it is known that lightweight flexible wing structures are potentially subjected to aeroelastic instabilities that limit their operative flight envelope. In order to extend the flight envelope of flexible wing structures the research is pushing on using active methods, i.e. control systems specifically designed for vibration suppression, instead of classical passive methods such as mass balancing and stiffness tailoring [1]. Over the years, many control algorithms have been proposed for flutter suppression systems purposes and applied to different aeroelastic plant numerical models, starting from the low-fidelity typical section [2, 3] to the higher fidelity finite element modeling coupled with aerodynamics panel methods [4]. In the recent years adaptive control algorithms are gaining increasing interest due to their ability to face the strong speed dependence of aeroelastic phenomena [5]; meanwhile, the possibility of using multiple control surface to extend the wing flutter boundary is starting to be explored to come up with more robust and reliable flutter suppression [6] and gust load alleviation systems [7, 8].

The aim of this work is to analyzethe possibility of using multiple trailing edge control surfaces for wing flutter suppression by comparing the results with a single aileron configuration. In order to carry out the comparative study an alternative aeroelastic beam finite element reduced order modeling approach is used and an adaptive control system architecture is implemented. The low order aeroelastic modeling proposed allows to obtain an efficient aero-servo-elastic analysis framework characterized by low computational costs, a highly sought feature for preliminary aeroelastic studies on the best control surfaces configuration.

2. Aeroelastic Plant modelling

The aeroelastic system consists of a wing with rectangular planform having a semi-span length l_w and semi-chord b. The wing features an aileron, hinged to the main wing structure, extending from a distance l_F from the wing's root to its tip. Additionally, the positions of the actuators, l_{a1} and l_{a2} , are defined with respect to the inboard aileron edge station l_F . The torsional elasticity of the aileron is taken into account, assuming it undergoes elastic deformations around the hinge. The wing is modeled as an equivalent beam, adhering to Euler-Bernoulli and De Saint Venant beam theories kinematics. The wing degrees of freedom include bending displacement w(x,t), torsional rotation $\phi(x,t)$, and control surface deflection $\delta(x,t)$, to which is added the aerodynamic lag state degree of freedom \bar{x} introduced by the time domain aerodynamic model [9]. A scheme of the wing is shown in Figure 1, where relevant geometric parameters are also depicted. In detail, the elastic axis distance from the mid-chord is ba, the center of gravity one is bx_ϕ , while bc denotes the aileron hinge line distance from the mid-chord and bx_δ its center of gravity distance from the hinge.

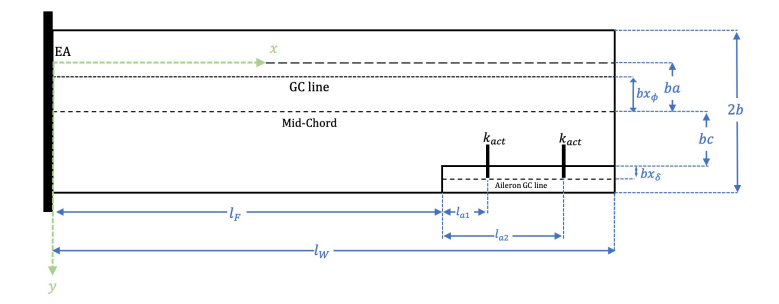


Figure 1 – Wing-aileron scheme

The aeroelastic beam formulation relies on the equivalent beam modeling of the structure and the Theodorsen aerodynamic model for oscillating airfoils. The wing equivalent beam is characterized by its bending stiffness EI and torsional stiffness GK, while the aileron is modeled as a torsion rod characterized by its torsional stiffness that is a combination of its elastic stiffness G_aK_a and the hinge stiffness K_δ . More in detail, the aileron hinge stiffness takes into account the actuators stiffness and reads as

$$K_{\delta} = k_{\delta} + k_{act} \delta_F \tag{1}$$

being k_{δ} the hinge stiffness per unit length and k_{act} the actuator stiffness; moreover, δ_F determines the actuator position, with respect to the inboard aileron edge, through the Dirac's delta function δ_d as $\delta_F = \delta_d (x - l_F - l_{a1}) + \delta_d (x - l_F - l_{a2})$.

The equivalent beam equations of motion are defined in a compact matrix form [9] introducing the generalized displacement vector $\mathbf{q}(x,t) = \begin{bmatrix} w & \phi & \delta & \vec{x} \end{bmatrix}^T$

$$[\mathbf{M}_s + \mathbf{M}_{aer}] \dot{\mathbf{q}}(x,t) + [\mathbf{C}_s + \mathbf{C}_{aer}] \dot{\mathbf{q}}(x,t) + [\mathbf{K}_s D^2 + \mathbf{K}_{\delta} + \mathbf{K}_{aer}] \mathbf{q}(x,t) = \mathbf{0}$$
(2)

being \mathbf{M}_s , \mathbf{M}_{aer} , \mathbf{C}_s , \mathbf{C}_{aer} , and \mathbf{K}_s , \mathbf{K}_{aer} the mass, damping, and stiffness matrices, where the subscripts s and aer stands for structural and aerodynamic, respectively. Moreover, D is a differential operator related to the derivatives along the beam axis and \mathbf{K}_{δ} is the aileron stiffness matrix that collects the hinge stiffness of eq. 1.

Writing eq. 2 in weak form and introducing the displacement field interpolation [9] the aeroelastic beam finite element matrices are computed as

$$\mathbf{M}_{e} = \int_{L} \mathbf{N}^{T} \left[\mathbf{M}_{s} + \mathbf{M}_{aer} \right] \mathbf{N} dx; \quad \mathbf{C}_{e} = \int_{L} \mathbf{N}^{T} \left[\mathbf{C}_{s} + \mathbf{C}_{aer} \right] \mathbf{N} dx; \quad \mathbf{K}_{e} = \int_{L} \left[(D\mathbf{N})^{T} \mathbf{K}_{s} D + \mathbf{N}^{T} \mathbf{K}_{\delta} + \mathbf{N}^{T} \mathbf{K}_{aer} \right] \mathbf{N} dx$$
(3)

Then, assembling the matrices according to the wing discretization, and imposing the cantilever boundary conditions, the discretized wing structural equations of motion are obtained

$$\begin{bmatrix} \mathbf{M}_{11} & \mathbf{M}_{12} \\ \mathbf{M}_{12}^T & \mathbf{M}_{22} \end{bmatrix} \begin{bmatrix} \ddot{\Delta}_1 \\ \ddot{\Delta}_2 \end{bmatrix} + \begin{bmatrix} \mathbf{C}_{11} & \mathbf{C}_{12} \\ \mathbf{C}_{12}^T & \mathbf{C}_{22} \end{bmatrix} \begin{bmatrix} \dot{\Delta}_1 \\ \dot{\Delta}_2 \end{bmatrix} + \begin{bmatrix} \mathbf{K}_{11} & \mathbf{K}_{12} \\ \mathbf{K}_{12}^T & \mathbf{K}_{22} \end{bmatrix} \begin{bmatrix} \Delta_1 \\ \Delta_2 \end{bmatrix} = \mathbf{0} \quad (4)$$

The state space form of eq. 4 is obtained introducing the state vector $X = \begin{bmatrix} \mathbf{\Delta}_1^T & \dot{\mathbf{\Delta}}_1^T \end{bmatrix}^T$, the dynamic matrix \mathbf{A} , and the state-input relation \mathbf{B} . In detail, \mathbf{B} is computed defining a submatrix \mathbf{K}^{δ}_{12} of \mathbf{K}_{12} corresponding to the aileron displacement at the actuator-aileron linking stations, that represent the plant inputs (collected in the input vector \mathbf{u}).

$$\mathbf{A} = \begin{bmatrix} 0 & I \\ -\mathbf{M}_{11}^{-1}\mathbf{K}_{11} & -\mathbf{M}_{11}^{-1}\mathbf{C}_{11} \end{bmatrix}; \quad \mathbf{B} = \begin{bmatrix} \mathbf{0} \\ -\mathbf{M}_{11}^{-1}\mathbf{K}^{\delta}_{12} \end{bmatrix}; \tag{5}$$

Last, the state-output matrix ${\bf C}$ is an identity matrix in the hypothesis of ideal sensors; therefore, the wing state space system reads as

$$\begin{cases} \dot{X} = \mathbf{A}X + \mathbf{B}\mathbf{u} \\ Y = \mathbf{C}X \end{cases} \tag{6}$$

3. Adaptive controller design

The adaptive control scheme considered in this work is based on a Simple Adaptive Controller (SAC). The SAC algorithm takes into account a reference model that generates the signal to be tracked by the controlled plant in order to let it follow the desired dynamics [10]. In detail, the SAC control signal is a linear combination of the reference model state, input, and of the tracking error e(t); however,in this work the control objective is to make the wing torsion angle zeroed,i.e. the desired value is $\phi_d = 0$, thus the SAC control law is reduced to the one presented in [11] only taking into account the wing torsion angle output signal $\phi(x,t)$ to compute the error e(t). In detail, $e(t) = 0 - \phi(l_w,t)$ in the single aileron configuration; while, for the double aileron configurations different driving signals (corresponding to different sensors location related to the torsion measurement at the actuator stations) for the SAC will be considered.

Being driven by the only torsion measurement of the wing, the output feedback adaptive control law reads as

$$u(t) = (K_{eP} + K_{eI}) e(t)$$
 (7)

where K_{eP} and K_{eI} are the controller adaptive gains expressed as

$$K_{eP}(t) = \Gamma_{eP}e^{2}(t)$$

$$\dot{K}_{eI}(t) + \eta K_{eI}(t) = \Gamma_{eI}e^{2}(t)$$
(8)

being Γ_{eP} and Γ_{eI} the invariant gains and η the lannou term that ensures the stability of the system when bounded disturbances are present [10].

However,it is to be stressed that the SAC algorithm can be only applied to systems that fulfill the passivity requirements [12]. In this work, a Parallel Feedforward Compensator (PFC) is added to the plant G(s), i.e the Single Input Single Output (SISO) transfer function related to Eq. 6, in order to make the system meet the Almost Strictly Positive Realness (ASPR) condition [13].It is worth to be

said that in the double aileron configuration studied in this work two SISO channels are identified, leading to the design of two independent control systems; thus, the passivity condition of each SISO transfer function has been studied separately and requested the implementation of a dedicated PFC. Note that the possible application of the SAC algorithm on isolated SISO channels of Multi Input Multi Output (MIMO) systems has been already verified in literature [14].

As presented in [15], the PFC is designed as the inverse of a controller H(s) that stabilize the closed loop system given by $G_c(s) = (1 + G(s)H(s))^{-1}G(s)$, being $H(s) = K_H(1 + \tau_H s)$ an ideal Proportional-Derivative (PD) controller. Thus, by adding the PFC output Y_{PFC} to the aeroelastic plant one, the augmented plant output Y_a can be used for feedback stabilisation through the SAC algorithm [16].

The SAC control system architecture for wing-aileron flutter suppression is shown in Figure 2, where the subscript *a* refers to the augmented plant variables.

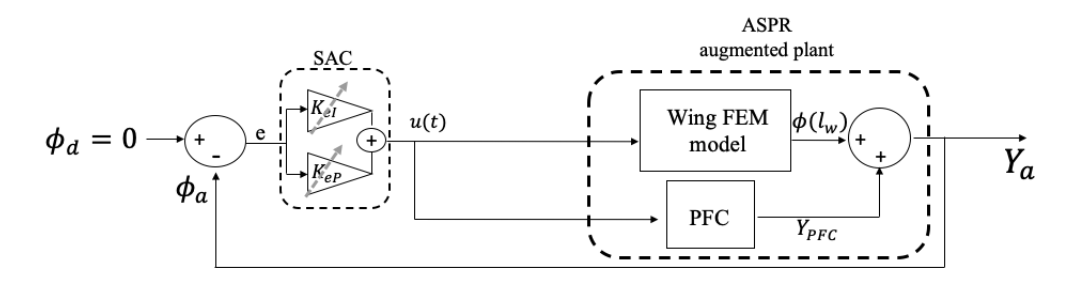


Figure 2 – Wing-aileron SAC flutter suppression architecture

The SAC parameters tuning is carried out by means of a Population Decline Swarm Optimization (P_DSO) algorithm [17]. The objective function of the optimization procedure is the Integral of Time Absolute Error (ITAE) [18] that reads as

$$ITAE = \int_{t_0}^{t_w} |e(t)| t dt$$
 (9)

being t_0 the initial perturbation time and t_w the simulation time. In this work, the values $t_0=0s$ and $t_w=1s$ have been defined. The particles coordinate vector P^i at each iteration λ is defined in the algorithm by the three SAC invariant parameters $P^i_{\lambda}=\left[\begin{array}{cc}\Gamma^i_{eP}&\Gamma^i_{eI}&\eta^i\end{array}\right]_{\lambda}$ and the optimization problem reads as

$$\min ITAE\left(P_{\lambda}^{i}\right)$$
s.t.
$$\Gamma_{eP_{\min}} \leq \Gamma_{eP} \leq \Gamma_{eI\max}$$

$$\Gamma_{eI_{\min}} \leq \Gamma_{eI} \leq \Gamma_{eI_{\max}}$$

$$\eta_{\min} \leq \eta \leq \eta_{\max}$$
(10)

where the research space boundaries have been defined within the ranges: $0 \le \Gamma_{Pe} \le 10^8$, $0 \le \Gamma_{Ie} \le 10^8$, $10^{-4} \le \eta \le 1$.

4. Results

The wing-aileron model considered in this work is a modification of the well-known Goland wing, studied in [19], which presents a trailing edge aileron extending from the 60% of the span to the wing tip. The wing and aileron parameters are reported in Table 1.

	Parameter	Value	Parameter	Value	Parameter	Value	Parameter	Value
Wing	<i>l</i> _w [m]	6.096	b [m]	0.914	а	-0.34	x_{ϕ}	-0.14
	r_{ϕ}	0.5	m_w [Kg/m]	35.71	$EI[Nm^2]$	$9.7722 \cdot 10^6$	$GK[Nm^2]$	$0.9876 \cdot 10^6$
Aileron	$l_F[m]$	0.6 l _w	l_{a1}	$0.25(l_w - l_F)$	l_{a2}	$0.75(l_w - l_F)$	$k_{\delta}[Nm/rad]$	0
	r_{δ}	0.1	m_f [Kg/m]	8.929	$G_a K_a [Nm^2]$	$1.42614 \cdot 10^3$	k_{act} [Nm/rad]	$6.48051 \cdot 10^3$
	c	0.6	x_{δ}	0.1				

Table 1 – Goland wing-aileron parameters

For the purposes of this work two configurations are considered, the original single-aileron one and a configuration for which the aileron is splitted in two ailerons with equal span. For the first comparison carried out in this section the actuators are located at the 70% and 90% of the wing span in both configurations.

From the carried out aeroelastic analysis it has been found that, according to [19], the flutter boundary is $v_f = 109.5 m/s$ and the flutter frequency is $\omega_f = 10.3 Hz$, these values are not affected by the aileron configuration, since the flutter mechanism only involves the first fundamental torsion and bending modes of the wing (see Figure 3).

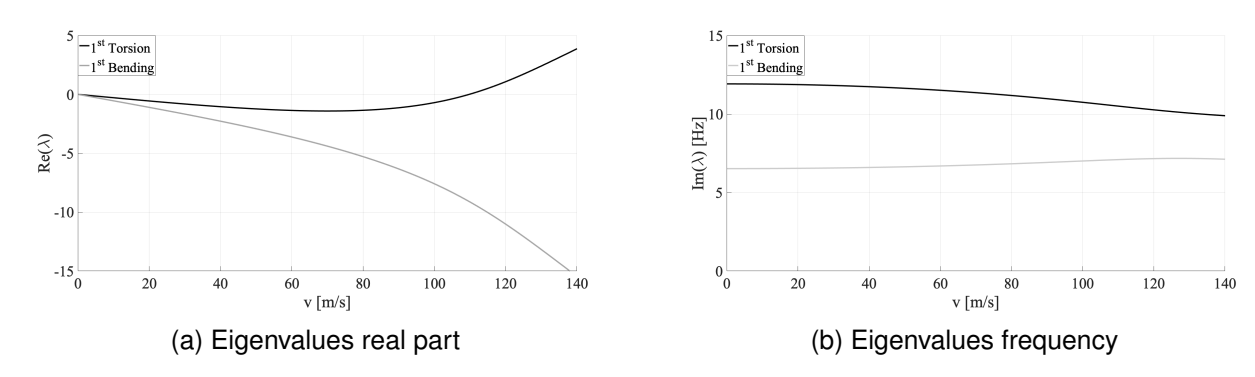


Figure 3 – Goland wing-aileron flutter diagrams

It is worth mentioning that the aeroelastic plant, i.e. the transfer function that relates the aileron displacement to the wing tip torsion angle, at the flutter speed is a marginally stable non-minimum phase system, thus the first step is the PFC design that makes the augmented plant ASPR. In order to design the PFC, the time constant of the PD controller has been fixed to $\tau_H = 10^{-3} s$ and the closed loop system poles have been computed for increasing gain values obtaining the results shown in Figures 4a - 4c - 4e for the single aileron configuration, inboard aileron, and outboard aileron, respectively. Then the gain values to be used have been chosen studying the augmented plant transfer function zeros for increasing free-stream velocities in order to find the higher speed range for which the augmented plant is ASPR. By a trial and error approach the best values of K_H have been found to be $K_H = \begin{bmatrix} 3 & 4.5 & 3.9 \end{bmatrix}$ for the single aileron configuration, inboard aileron, and outboard aileron. From Figures 4b - 4d - 4f it can be observed that the passivity condition is satisfied for velocities below the values $v_f = \begin{bmatrix} 171 & 190.6 & 193.7 \end{bmatrix} m/s$, that represent the ideal closed loop systems flutter boundary. Therefore, from the results obtained it can be said that the subdivision of the aileron in two separated control surfaces allows to extend the passivity range of the 11.46%.

Single Aileron							
	$\Gamma_{Pe}\left[1/rad^2\right]$	$\Gamma_{Ie} \left[s/rad^2 \right]$	$\eta \left[s^{-1} \right]$				$ITAE[rad \cdot s]$
	$3.046 \cdot 10^6$	304	10^{-3}				$3.46 \cdot 10^{-3}$
	Double	Aileron					
	$\Gamma_{Pe}^{in} \left[1/rad^2 \right]$	$\Gamma_{Ie}^{in} \left[s/rad^2 \right]$	$\eta^{in} \left[s^{-1} \right]$	$\Gamma_{Pe}^{out}\left[1/rad^2 ight]$ 930	$\Gamma_{Ie}^{out} \left[s/rad^2 \right]$	$\eta^{out} \left[s^{-1} \right]$	$ITAE[rad \cdot s]$
	825	$1.130 \cdot 10^6$	10^{-3}	930	$9.55 \cdot 10^4$	10^{-3}	$1.77 \cdot 10^{-3}$

Table 2 – Optimized SAC invariant gains

Once the PFC have been designed, the SAC invariant gains tuning has been carried out using the P_DSO algorithm that aims at minimizing the ITAE of the wing tip torsion angle time history, considering that the wing is subjected to a pulse disturbance on the torsion rate with amplitude $\dot{\phi}(0) = 100 rad/s$ occurring at time instant t=0 and with width $t_{pulse}=0.001s$. More details on the optimization procedure can be found in [16]. The optimization resulted in the SAC invariant gains sets resumed in table 2 where the superscripts in and out, refer to the inboard and outboard aileron control systems in the double configuration, respectively. Looking at the optimized gains it can be observed that the subdivision of the aileron in two independent control surfaces leads to a greater relevance of the integral

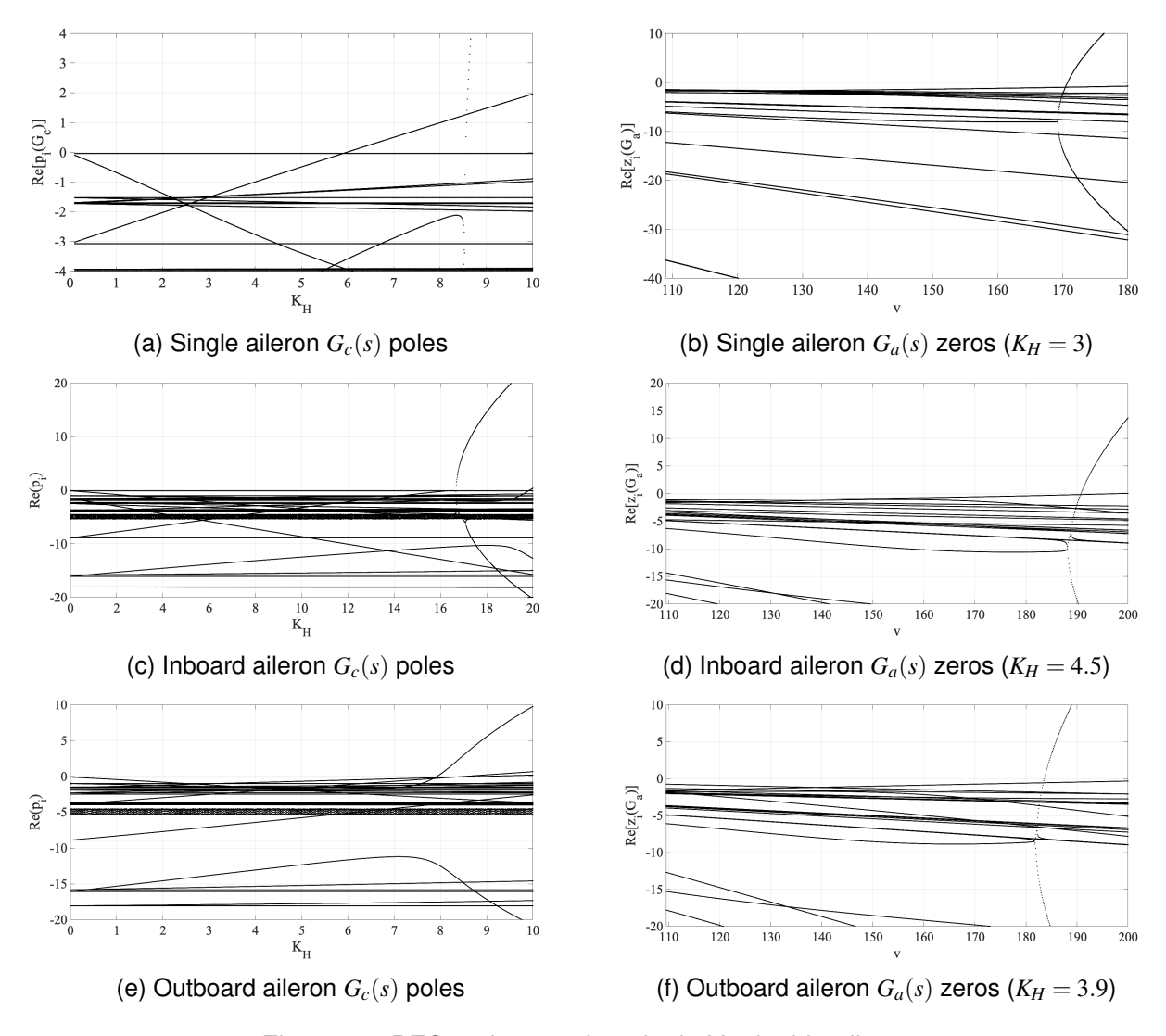


Figure 4 – PFC tuning results: single Vs double aileron

contribution in the SAC algorithm, while the proportional contribution tends to lower values.

The optimized invariant gains of Table 2 have been used to simulate a flight scenario equivalent to the one used for the optimization, but considering that for the initial 0.5 seconds the flutter suppression systems are turned off, allowing the aeroelastic plant to reach the self-sustained oscillations condition after the pulse disturbance. The obtained results are shown in Figure 5, where it can be observed that, simply dividing the aileron in two independent control surfaces, there is not a relevant change in the overall system vibrations trends; anyway, the high frequency fluctuations that appears in the single aileron configuration, are greatly reduced due to the change in stiffness and inertia in the separated control surfaces case. This high frequency fluctuations mitigation represents on its own an enhancement on the dynamic behavior of the structure; in fact, by experiencing lower vibration cycles the structure is less subjected to fatigue phenomena and control surfaces hinge wear. Moreover, it is to be noted that the commanded deflections of the two ailerons do not present any phase lag, but only a slight difference in magnitude (the outboard aileron being higher); this behavior is expected since the only signal that drives both control systems is the wing tip torsion measurement.

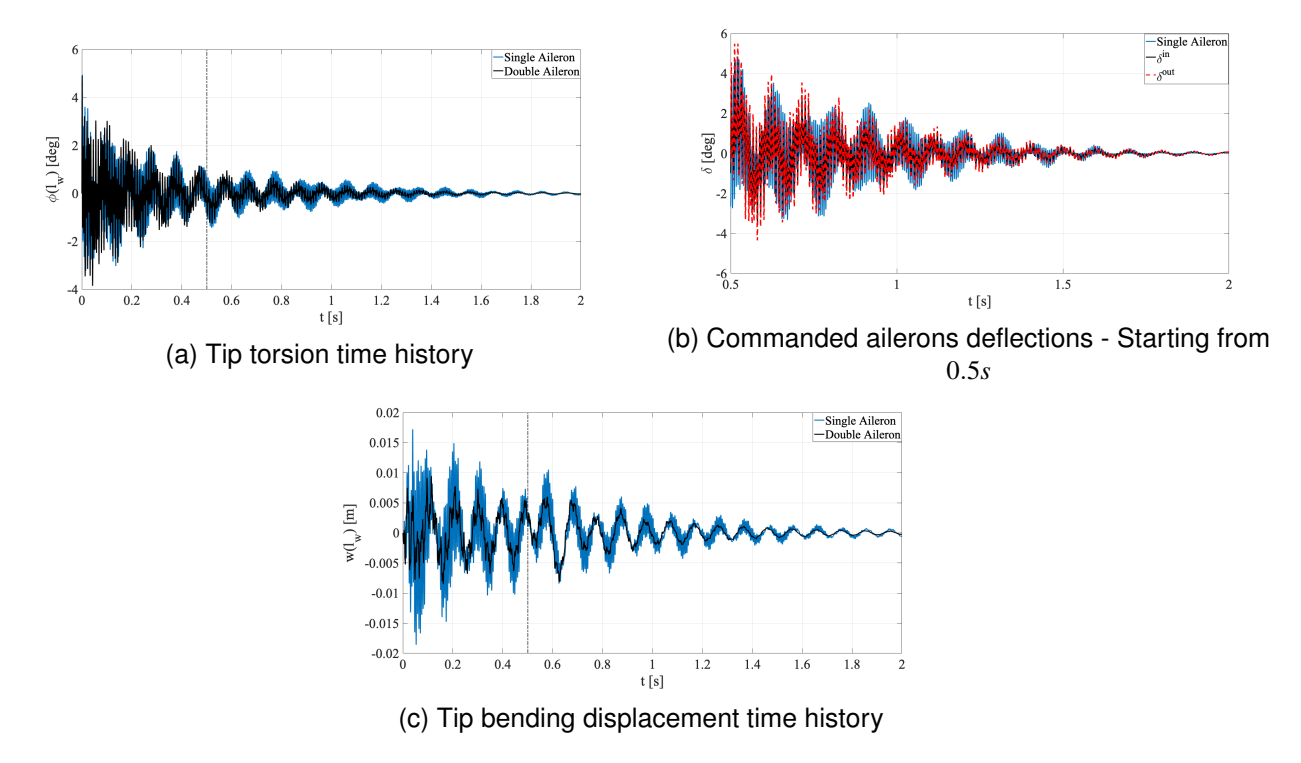


Figure 5 – Flutter speed responses: single Vs double aileron

A second comparison has been carried out considering two splitted aileron configurations. In detail, for these configurations, the SAC algorithm on each aileron is driven by the torsion measurement at the wing station on which the actuator apply. In the first case study the actuators are still located at the 70% and 90% of the wing span , i.e at the centre of each aileron, while in the second case the actuators are moved at each aileron inboard edge. These variants allows to study the influence of both sensor and actuators location on the flutter suppression system performance.

As done for the first case studies presented in this section, the first step has been the PFC tuning. The time constant of the PD controller has been fixed to $\tau_H = 10^{-3} s$ in this case, too; thus, the closed loop system poles have been computed for increasing gain values obtaining the results reported in Figure 6, where it can be observed that implementing the local torsion measurements improves the maximum stabilizing gain for $G_c(s)$ in both actuators placement configurations. The best values of K_H have been again found by a trial and error procedure, resulting in $K_H = [9.5 \quad 3.9]$ for the middle actuator case and $K_H = [9.5 \quad 6.3]$ for the inner edge actuator one. Therefore, looking at the evolution of the augmented plant zeros it is found that the passivity condition is fulfilled until the air-stream velocities $v_f = [179.3 \quad 195.2] \, m/s$ and $v_f = [178.9 \quad 195.8] \, m/s$ in each case. From the results obtained, it can be noted that, in the splitted aileron configuration, by considering the local torsion deformation of the wing at the actuators station the flutter boundary extension is reduced for the inboard aileron control system with respect to the case in which it is related to the wing tip.

5. Conclusions

In this work the application of adaptive flutter suppression systems to a wing equipped with a single or double aileron has been studied. The numerical model of the wing has been obtained by means of an aeroelastic beam finite element modelling approach and a simple adaptive control scheme has been implemented to realize the adaptive flutter suppression systems. Different placement of the ailerons actuators and sensors have been studied in order to find the best configuration in terms of flutter boundary extension for the structure. From the analyses carried out it has been found that the double aileron configuration improves the adaptive flutter suppression system performance, with respect to the single aileron one, and that the best arrangement relies on the torsion measurements at the wing tip with actuators placed at the mid-span of each aileron.

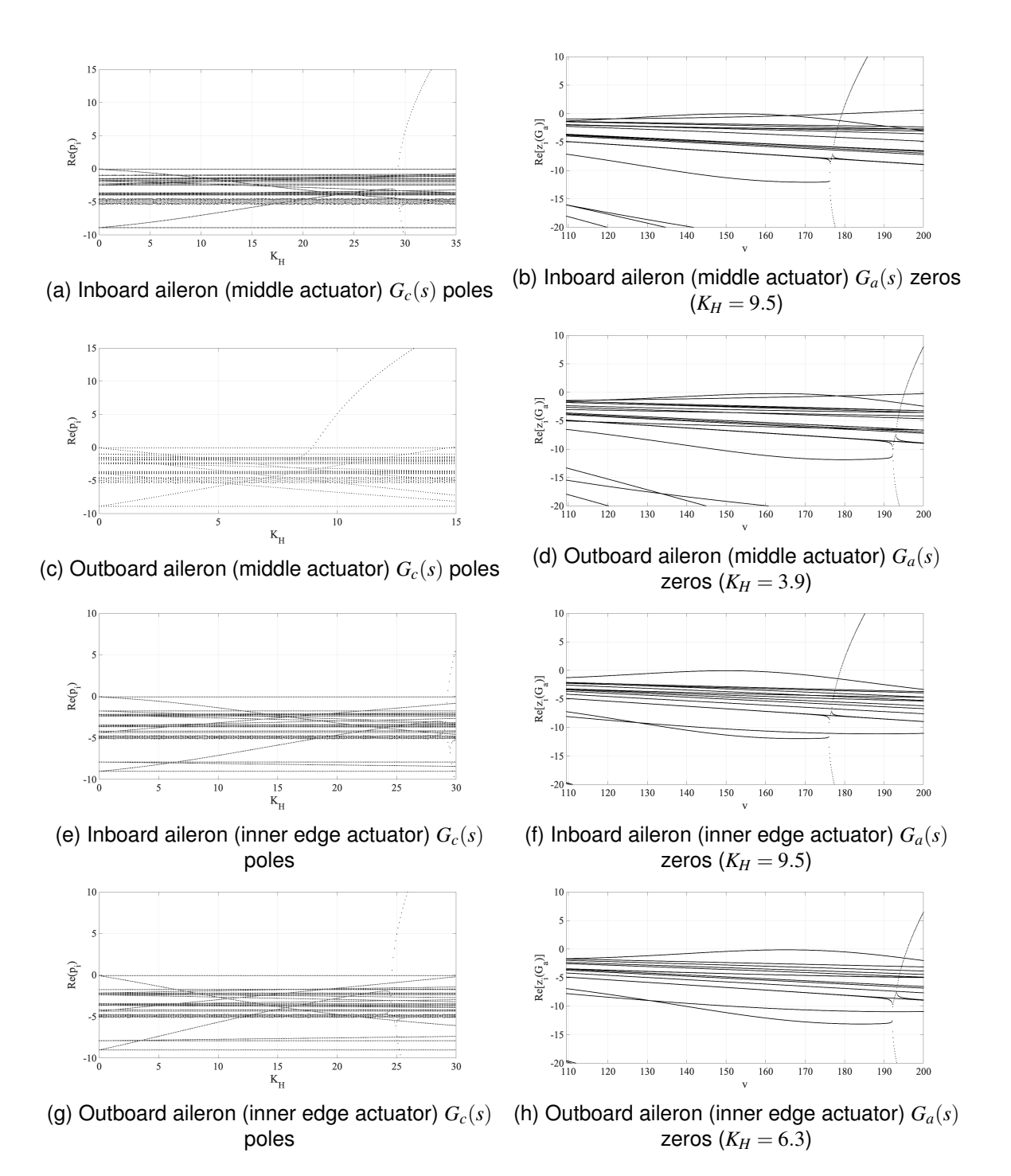


Figure 6 – PFC tuning results: middle actuator Vs inner edge actuator

6. Contact Author Email Address

mailto: carmelorosario.vindigni@unikore.it

7. Copyright Statement

The authors confirm that they, and/or their company or organization, hold copyright on all of the original material included in this paper. The authors also confirm that they have obtained permission, from the copyright holder of any third party material included in this paper, to publish it as part of their paper. The authors confirm that they give permission, or have obtained permission from the copyright holder of this paper, for the publication and distribution of this paper as part of the ICAS proceedings or as individual off-prints from the proceedings.

Aknowledgments

The study was financially supported by the Italian Ministry of University and Research - M.U.R. under the DAVYD project (P.O.N. Grant ARS01_00940).

References

- [1] E. Livne, "Aircraft active flutter suppression: State of the art and technology maturation needs," *Journal of Aircraft*, vol. 55, no. 1, pp. 410–452, 2018.
- [2] T. Theodorsen, "General theory of aerodynamic instability and the mechanism of flutter," tech. rep., 1949.
- [3] D. A. Peters, M.-c. A. Hsieh, and A. Torrero, "A state-space airloads theory for flexible airfoils," *Journal of the American Helicopter Society*, vol. 52, no. 4, pp. 329–342, 2007.
- [4] E. Albano and W. P. Rodden, "A doublet-lattice method for calculating lift distributions on oscillating surfaces in subsonic flows.," *AIAA journal*, vol. 7, no. 2, pp. 279–285, 1969.
- [5] C. R. Vindigni, A. Esposito, and C. Orlando, "Stochastic aeroservoelastic analysis of a flapped airfoil," *Aerospace Science and Technology*, vol. 131, p. 107967, 2022.
- [6] S. Waitz, "Active flutter suppression of a highly flexible swept wing through multiple flap control," 2022.
- [7] H. Fournier, P. Massioni, M. Tu Pham, L. Bako, R. Vernay, and M. Colombo, "Robust gust load alleviation of flexible aircraft equipped with lidar," *Journal of Guidance, Control, and Dynamics*, vol. 45, no. 1, pp. 58–72, 2022.
- [8] L. Zhang and Y. Zhao, "Adaptive feed-forward control for gust load alleviation on a flying-wing model using multiple control surfaces," *Aerospace*, vol. 10, no. 12, p. 981, 2023.
- [9] C. R. Vindigni, G. Mantegna, A. Esposito, C. Orlando, and A. Alaimo, "An aeroelastic beam finite element for time domain preliminary aeroelastic analysis," *Mechanics of Advanced Materials and Structures*, vol. 30, no. 5, pp. 1064–1072, 2023.
- [10] I. Barkana, "Simple adaptive control—a stable direct model reference adaptive control methodology—brief survey," *International Journal of Adaptive Control and Signal Processing*, vol. 28, no. 7-8, pp. 567–603, 2014.
- [11] A. L. Fradkov, I. V. Miroshnik, and V. O. Nikiforov, *Nonlinear and adaptive control of complex systems*, vol. 491. Springer Science & Business Media, 2013.
- [12] I. Barkana, "Robustness and perfect tracking in simple adaptive control," *International Journal of Adaptive Control and Signal Processing*, vol. 30, no. 8-10, pp. 1118–1151, 2016.
- [13] I. Rusnak and I. Barkana, "Spr and aspr untangled," *IFAC Proceedings Volumes*, vol. 42, no. 6, pp. 126–131, 2009.
- [14] O. I. Borisov, A. A. Bobtsov, A. A. Pyrkin, and V. S. Gromov, "Simple adaptive control for quadcopters with saturated actuators," in *AIP Conference Proceedings*, vol. 1798, p. 020031, AIP Publishing LLC, 2017.
- [15] C. R. Vindigni and C. Orlando, "Simple adaptive v-stack piezoelectric based airfoil flutter suppression system," *Journal of Vibration and Control*, vol. 29, no. 11-12, pp. 2802–2816, 2023.
- [16] C. R. Vindigni, G. Mantegna, C. Orlando, and A. Alaimo, "Simple adaptive wing-aileron flutter suppression system," *Journal of Sound and Vibration*, vol. 570, 2024.
- [17] A. Alaimo, A. Esposito, and C. Orlando, "P d so tuning of pfc-sac fault tolerant flight control system," *Advances in aircraft and spacecraft science*, vol. 6, no. 5, pp. 349–369, 2019.
- [18] M. I. Solihin, L. F. Tack, and M. L. Kean, "Tuning of pid controller using particle swarm optimization (pso)," in *Proceeding of the international conference on advanced science, engineering and information technology*, vol. 1, pp. 458–461, 2011.
- [19] S. Mozaffari-Jovin, R. Firouz-Abadi, and J. Roshanian, "Flutter of wings involving a locally distributed flexible control surface," *Journal of Sound and Vibration*, vol. 357, pp. 377–408, 2015.